Journal of CO2 Utilization 70 (2023) 102458

Contents lists available at ScienceDirect

Journal of CO2 Utilization

journal homepage: www.elsevier.com/locate/jcou

Effectiveness of the 3D-printing procedure in the synthesis of hybrid catalysts for the direct hydrogenation of CO_2 into dimethyl ether

G. Bonura [a,*], S. Todaro [a], V. Middelkoop [b], Y. de Vos [b], H.C.L. Abbenhuis [c], G. Gerritsen [c], A.J.J. Koekkoek [c], C. Cannilla [a], F. Frusteri [a]

[a] CNR-ITAE, Istituto di Tecnologie Avanzate per l'Energia "Nicola Giordano", via S. Lucia sopra Contesse 5, Messina 98126, Italy
[b] VITO, Vlaamse Instelling voor Technologisch Onderzoek, Boeretang 200, Mol 2400, Belgium
[c] Hybrid Catalysis BV, Den Dolech 2, 5612 AZ, Eindhoven, the Netherlands

ARTICLE INFO

Keywords:
3D-catalysts
CCU
Catalytic hydrogenation
Dimethyl ether
Hybrid catalysts

ABSTRACT

This work highlights the effectiveness of an unconventional synthesis of hybrid systems for the direct hydrogenation of carbon dioxide into dimethyl ether (DME), based on micro-extrusion of a ink-like catalytic paste by a robocasting procedure. Due to the possibility to exert a fine control over the structure, surface and geometric architecture, the adopted printing technique really ensures a superior management of heat and mass constraints in respect of the conventional powdered catalysts, the catalyst functionality resulting to be tightly dependent on the cooperation between metal-oxide and acidic phase. Additionally, the accessibility both of the CO_2 activation and methanol (MeOH) dehydration sites over the hybrid micro-extruded catalyst most importantly affects the catalytic performance, as suggested by the values of turnover frequency of CO_2 conversion and DME formation pointing out the need for a favorable exposure of chemisorption sites of different nature to enhance the specific reactivity.

1. Introduction

The combustion of fossil fuels for energy production releases into the atmosphere a large amount of CO_2 which is claimed as a main cause of the greenhouse effect [1–4]. The commitment of the International governments to mitigate the inherent issues has recently driven 195 Parties setting new targets during the 27th UN Climate Change Conference (COP27, Sharm el-Sheikh 2022) to reach zero emissions by 2050 and to keep global warming below 1.5 °C.

Furthermore, the energy crisis in Central and Eastern Europe poses the need for searching safe alternatives to energy supply to give immediate and practical answers to the contingent needs. From this point of view, the technologies related to Carbon Capture and Utilization (CCU) are arousing a strong interest, for the possibility to close the carbon loop by an effective recycling of CO_2 captured either directly from the air or from industrial power plants, then reusing it in presence of renewable hydrogen for the production of value-added products [5–8].

Dimethyl ether (DME) has been getting growing attention as an alternative diesel fuel and also as a feedstock for producing versatile chemicals and fuels, such as light olefins, methyl acetate, dimethoxyethane, etc [9–13]. Conventionally DME is synthesized starting from syngas in two steps, involving first the formation of methanol over a multi-metallic catalyst and then the dehydration of methanol to DME over solid acid systems [14–20]. The final productivity is controlled by the rate of methanol synthesis, in turn limited by thermodynamic constraints, feed composition, extent of the recycling stream [21,23]. The direct synthesis of DME taking place in a single reactor from either $CO/CO_2/H_2$ or CO_2/H_2 mixtures can overcome these limitations, leading to higher DME productivity owing to a more favourable equilibrium conversion prompted by the continuous consumption of methanol initially formed [20–22,24–26]. However, this one-step process has not reached an industrial maturity yet, being still performed on a lab-scale in presence of a hybrid metal-oxide-acid catalyst.

Typically, copper-based ternary systems, such as $CuO\text{-}ZnO\text{-}Al_2O_3$ or $CuO\text{-}ZnO\text{-}ZrO_2$, are integrated with solid acidic phases, like $\gamma\text{-}Al_2O_3$ or zeolite materials [23–31], active in the dehydration of methanol. The extent of the interface area among different phases leading to an effective interaction, the proximity of catalytic sites of different nature preventing a measurable mass diffusion control, the sample reproducibility

* Corresponding author.
E-mail address: giuseppe.bonura@itae.cnr.it (G. Bonura).

https://doi.org/10.1016/j.jcou.2023.102458
Received 31 January 2023; Received in revised form 4 March 2023; Accepted 9 March 2023
Available online 14 March 2023

overcoming the complexity in controlling several variables during preparation, the need for a stable lifetime under the adopted experimental conditions, represent all challenging factors requiring further R&D for an industrial process scalability.

Among variously shaped solid catalysts (e.g., powders, beads, granules, pellets, scaffolds), matrix-like structures with different geometry of channels and typically prepared by impregnation or washcoating have been demonstrated to be promising systems for various catalytic processes [32–38], offering many benefits in terms of control of the sample architecture, increase of mass and heat transfer, decrease of pressure drops and related costs of process management. Nevertheless, their specific utilization in CCU applications results to be scarcely documented yet, now receiving a decisive boost by the recent progresses in the three-dimensional (3D) printing techniques, expected to revolutionize in the short term all the sectors of research and industry and to have implications on the concepts of production and work too, with economic and ethical consequences [39,40]. 3D Printing, also referred as "additive manufacturing" (AM), designates a technology suitable to build a material directly from a virtual 3D model by overlapping layers of the same material. In general, to produce a piece by 3D printing is sufficient the choice of a 3D software, a 3D model and a starting material. Consequently, it is possible to generate parts with arbitrary geometries without the need to adopt the usual productive processes bound to mass production [41,42]. The pieces thus created are ready for use, not requiring other finishing treatments, as well as the manufacture of semi-finished components results to be economically profitable. The starting material in the process is typically used in the form of a powder, paste, ink, suspension or solid in an optimized phase for layered deposition.

Among the AM methods more and more importantly impacting the sector of the 3D printing, the direct-ink-writing (DIW), or robocasting, offers the superior potential not only for the realization of purely ceramic [43,44], but also of metallic or hybrid materials [45–50]. Its strong point is the relatively low cost of the machine, which normally uses an ink paste with specific rheological and viscosity features due to the addition of binders or additives in the parent material. This technology uses an extrusion process through a nozzle which generally varies from 0.1 to few millimeters, from which the material comes out in the form of a continuous filament which is deposited in superimposed layers through the control of a system robot, following a path generated starting from a suitably designed 3D model. Therefore, in a robocasting procedure, a 3D model is layered similar to other additive manufacturing techniques, but the nozzle position is controlled, extrapolating the shape of each layer by a CAD model. The first part of a product made by robocasting is obtained by extruding the "ink" threads onto the first layer. Subsequently, the working area is moved down or the formation hole rises and the next layer is applied to the required position. This is repeated until the product is completed.

In this work, the effectiveness of structured catalysts, prepared via robocasting in the form of matrix-like cylinders, was evaluated as viable alternative to conventional powdered catalysts for the development of a scalable CO_2 hydrogenation technology for the direct synthesis of DME. The physico-chemical and catalytic properties come out upon the robocasting procedure were compared with their powdered counterparts, in order to understand the key aspects behind a 3D-printing technique in the preparation of effective materials for CCU applications.

2. Experimental

2.1. Catalyst preparation

The composition of the ink-pastes to be micro-extruded by 3D printing was based on a 85 wt% dry content basis of a previously optimized hybrid CuO-ZnO-ZrO_2/zeolite formulation, well diluted (ca. 15 wt%) by an inorganic silica-based binder. In particular, the hybrid paste was preliminarily prepared via slurry coprecipitation of nitrate metal precursors, in a relative atomic ratio Cu/Zn/Zr of 60/30/10, by adding a suitable amount of oxalic acid to an ethanolic slurry solution containing a calculated amount of a commercial MFI-type zeolite (*Alfa Aesar*, Si/Al=25 mol/mol) so to get a final CuO-ZnO-ZrO_2:zeolite weight ratio of 1:1. The hybrid coprecipitated catalyst was then dried overnight, calcined at 500 °C for 4 h, before undergoing the mixing with the binder for printing. The micro-extrusion process was carried out through a customized LUTUM® 3D clay printer, by setting specific printing parameters in relation to the ink paste viscosity, with nozzles diameters of few hundreds of micron and stack layers in controlled patterns according to the desired architecture. After printing, the cylinders were dried in a humidity chamber at 25 °C for two days until conferring a firm structure. Afterwards, the dried monoliths were calcined by applying a slow heating rate of 1 °C/min until 500 °C under a helium atmosphere (100 *STP* mL min^{-1}).

A powdered hybrid CuO-ZnO-ZrO_2/MFI catalyst (Hyb-pwd), prepared by conventional coprecipitation with a Cu/Zn/Zr ratio of 60/30/10 at/at and a metal-oxide(s)-to-zeolite ratio of 1:1 wt/wt, was taken as a reference [20].

2.2. Sample characterization

The elemental composition of catalysts was determined by X-ray fluorescence analysis, using a S8 TIGER spectrometer (Bruker AXS, Germany), equipped with a rhodium anode tube (power 4 kW and 75 μm Be window and LiF 220 crystal analyze). The samples were analyzed as loose powders, considering the emission transitions of copper, zinc and zirconium (Cu-Kα1, Zn-Kα1, Zr-Kα1).

The crystallinity of the prepared samples was analyzed upon crushing by a *D8 Advance* diffractometer (Bruker AXS, Germany), operating with a Ni *b*-filtered Cu-Kα radiation (λ = 1.5406 Å) in the *2θ* range 5–80° at 40 kV and 40 mA and a scan step of 0.03° s^{-1}.

The measurements of reducibility under hydrogen atmosphere (TPR) were performed in a linear quartz micro-reactor (i.d., 4 mm) fed with a 5.6 vol% H_2/Ar mixture at the flow rate of 60 STP mL/min. The experiments were carried out in the range 0–800 °C with a heating rate of 12 °C/min. The hydrogen consumption was monitored by a thermal conductivity detector, calibrated by the peak area of a known amount of CuO. TPR data resulted very reproducible in terms both of maximum position (± 3 °C) and extent of H_2 consumption (± 3%).

The copper surface area (S_{Cu}) was obtained by "single-pulse" N_2O-titration measurements at 90 °C. Preliminarily the samples were reduced in situ at 300 °C in flowing H_2 (100 *STP* mL/min) for 1 h, then "flushed" at 310 °C in nitrogen carrier flow (15 min) and further cooled down at 90 °C. The values of metallic area were calculated assuming a Cu:N_2O= 2:1 titration stoichiometry and a surface atomic density of 1.46×10^{19} Cu_{at}/m^2.

A stereomicroscope Nikon® SMZ1500, with a zoom ratio of 15–1 accounting for a total magnifying capability of 3.75x up to 540x, was coupled to a Coolpix 5400 digital camera to carry out the high-resolution study of the printed structure of the samples.

Measurements of temperature-programmed desorption of carbon dioxide (CO_2-TPD) and ammonia (NH_3-TPD) were performed in the experimental setup used for TPR to determine the surface concentrations of base and acidic sites respectively. Before TPD experiments, the catalyst samples (~100–200 mg) were pre-reduced in a linear quartz micro-reactor (*l.*, 200 mm; *i.d.*, 4 mm) at atmospheric pressure, by flowing hydrogen (100 *STP* mL/min) from room temperature to 300 °C (heating rate of 10 °C/min). After an isothermal step of 60 min at 300 °C under hydrogen flow, followed by purging with helium, the samples were saturated for 60 min at 200 °C in a gas mixture (flow rate of 50 mL/min) either of 20 vol% CO_2/He or 5 vol% NH_3/He. Then, the samples were cooled down to 100 °C in He flow until a constant baseline level was maintained. The desorption measurements were carried out in a range from 100° to 600°C, at a heating rate of 12 °C/min, using helium as the carrier flow (50 *STP* mL/min). CO_2 (*m/z*, 44) or NH_3 (*m/z*, 17)

desorption process was monitored by a quadrupole mass spectrometer (*Thermo*^{Star}) equipped with a heated (150 °C) fast-response inlet capillary system, quantitatively calibrated by known pulses of CO_2 or NH_3.

2.3. Catalytic testing

In order to operate under a similar residence time without any control due to possible mass and heat diffusion resistances, two differently sized fixed bed stainless steel reactors were adopted either for the catalytic measurements with the 3D sample (*i.d.*, 12.8 mm; *l.*, 400 mm) or the powdered sample (*i.d.*, 6.4 mm; *l.*, 400 mm) respectively, being jacketed within a stainless steel rod to maintain an effective control of temperature during the run. The 3D monoliths were reduced in situ at 300 °C for 1 h under a "pure" hydrogen flow at atmospheric pressure. The catalytic data were achieved at 30 bar, in a range of temperature between 200 and 260 °C, under CO_2-to-DME hydrogenation conditions by feeding a mixture of $CO_2/H_2/N_2$ at a volumetric ratio of 3/9/1, operated at a space velocity of 1000 *NL*/kg_{cat}/h. The reaction stream was analyzed by a GC equipped with a two-column separation system connected to a flame ionized detector (FID) and a thermal conductivity detector (TCD), respectively. Both internal standard and mass-balance methods were adopted for the calculation of conversion-selectivity data, with an accuracy of ± 3% and carbon balance close to 100%.

3. Results and discussion

Fig. 1-A) displays the digital image of the micro-extruded matrix-like sample. It should be noted that the calcined cylinder typically presented an external diameter of 12.5 mm suitable to fit the inner diameter of the reactor. In particular, the top-view image in Fig. 1-B) reveals the uniform square channel cross-section of the structures with the wall thickness of ~0.65 mm and channel width of ~0.4 mm.

Both the XRD patterns of the printed and powdered samples, after the reduction treatment, are shown in Fig. 2. As it can be observed, not only the reflections of the MFI framework of the HZSM-5 structure (JCPDS 38–0246), but also the crystallinity of the metallic phase of copper at 43° (JCPDS 01–089–2838), were retained after the three dimensional method.

Regarding other main catalyst features, Table 1 reports a comparison of the main physico-chemical properties determined for the printed (Hyb-3D) and the powdered sample (Hyb-pwd).

As it is possible to observe, the printing procedure really allows a perfect control of the catalyst properties, considering that in terms of composition (from XRF analysis), texture (values of surface area) and metallic properties (TPR and N_2O chemisorption) the Hyb-3D sample practically mirrors the features of the Hyb-pwd sample prepared by conventional coprecipitation.

The only differences are visibly associated to the surface properties, as the result of a relatively lower acid-base capacity exhibited by the printed sample. Despite similar desorption profiles of the two samples both in terms of surface sites and temperatures of maximum desorption (not shown for the sake of brevity), the quantitative data reported in Table 1 show that the Hyb-3D sample exhibits not only a smaller CO_2 uptake (0.089 mmol/g_{cat}), but also a comparably smaller NH_3 uptake (0.362 mmol/g_{cat}), both values resulting ca. 50% than in the counterpart (0.178 mmol/g_{cat} and 0.721 mmol/g_{cat} for CO_2 uptake and NH_3 uptake respectively). Even without any distinction between Brønsted or Lewis sites, however the desorption profiles clearly suggest, on one hand, the presence of sites of same nature (although quantitatively different) and, on the other hand, how in presence of a multi-site surface the acid-base capacity is significantly dependent on the preparation procedure. Evidently, the intrinsic thermofluidic properties of the catalytic ink-paste prepared for the process of micro-extrusion (as related to the use of binders and additives for proper rheological features [44–46]), significantly controls the surface affinity of the chemisorption sites, namely basic CO_2 activation sites at the metal-oxide(s) surface and acidic dehydration sites at the zeolite surface [23,26,46,47]. Anyhow, the CO_2/NH_3 uptake ratio, taken as an index of relative concentration of the acid/base population, results to be practically identical on both samples (246.1–247.2), suggesting the same balance of acid-base population directly affecting the CO_2 activation process as well as the final step of methanol dehydration into DME.

Regarding the catalytic behavior, in Table 2 the catalytic results obtained in the direct hydrogenation of CO_2 to DME are reported, in terms of CO_2 conversion (X_{CO2}, %), selectivity to the various compounds (S_i, %) and yield to DME (Y_{DME}, %), in the temperature range

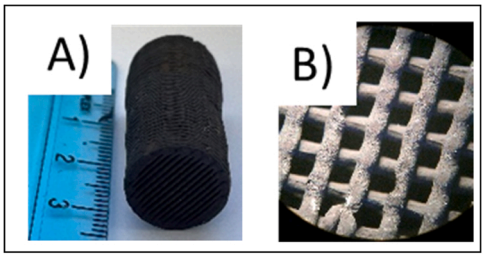

Fig. 1. Side-view (A) and top-view (B) of the printed Hyb-3D catalyst.

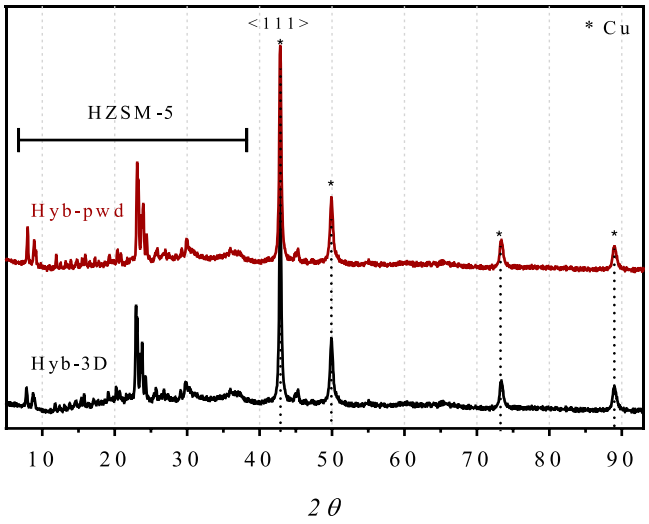

Fig. 2. XRD patterns of the Hyb-pwd and Hyb-3D samples after reduction.

Table 1
Main physico-chemical properties determined for the investigated samples.

Catalyst sample	Cu/Zn/Zr [a] (at %)	*SA* [b] (m^2/g)	H_2 cons. [c] ($mmol_{H2}/g_{cat}$)	S_{Cu} [d] (m^2/g)	CO_2 uptake [e] (mmol/g_{cat})	NH_3 uptake [f] (mmol/g_{cat})	CO_2/NH_3 [g]
Hyb-3D	61/31/9	251.8 ± 2.3	4.1	19.7	0.089	0.362	246.1
Hyb-pwd	60/30/10	248.1 ± 3.0	3.9	20.3	0.178	0.721	247.2

[a] Analytical composition from XRF analysis
[b] Surface Area from Langmuir method
[c] H_2 consumption from TPR measurements
[d] Copper surface area from N_2O chemisorption
[e] Cumulative basicity in the range 100–800 °C
[f] Cumulative acidity in the range 100–800 °C
[g] Basicity-to-acidity uptake ratio

Table 2
Catalytic data (X_{CO2}-S_{DME}-S_{MeOH}-S_{CO}) in the direct synthesis of DME from CO_2 hydrogenation at different temperatures (P_R, 3.0 MPa; $CO_2/H_2/N_2$, 3/9/1 v/v; *GHSV*: 1000 *N*L/Kg_{cat}/h).

Catalyst sample	T_R, 200 °C	T_R, 220 °C	T_R, 240 °C	T_R, 260 °C
	X_{CO2}–S_{DME}–S_{MeOH}–S_{CO} (%)	X_{CO2}–S_{DME}–S_{MeOH}–S_{CO} (%)	X_{CO2}–S_{DME}–S_{MeOH}–S_{CO} (%)	X_{CO2}–S_{DME}–S_{MeOH}–S_{CO} (%)
Hyb-3D	4.9–51.6–18.8–29.6	9.8–42.5–12.2–45.3	16.7–39.5–11.2–49.3	22.8–36.0–10.9–53.1
Hyb-pwd	11.0–51.2–12.5–36.3	16.4–49.0–11.0–40.0	22.0–47.4–13.0–39.6	23.6–42.6–13.7–43.7

220–260 °C, 30 bar and space velocity of 1000 *N*L/kg_{cat}/h.

As a rule, irrespective of the sample considered, the CO_2 conversion progressively increases with temperature, the highest values (22.8–23.6%) being attained at 260 °C, as leveled in proximity of the thermodynamic equilibrium [15]. At lower temperature, however, the sample Hyb-pwd exhibits a relatively higher activity as much higher as more determinant is operation under a pure kinetic regime (200–220 °C). In terms of product distribution, on each catalyst the DME selectivity regularly decreases with temperature, the trend resulting more marked on the 3D sample (51.6→36.0%) compared to the trend exhibited by the powdered catalyst (51.2→42.6%). On the other hand, despite a progressive increase on both samples, the CO selectivity more steeply rises on the Hyb-3D catalyst from 29.6% (at 200 °C) up to 53.1% (at 260 °C), against a less limited increase (36.3→43.7) exhibited by the Hyb-pwd sample in the range of temperature considered. Regardless of the reaction temperature, the MeOH selectivity remains almost stable and comparable (11.0–13.7%) on both systems, apart from a maximum value of 18.8% recorded for the printed sample at 200 °C.

It is clear that, with similar composition, texture and metallic features, the observed differences in the activity-selectivity pattern of the investigated samples have been primarily associated to their different surface properties as induced by the preparation method. Accordingly, to confirm the control of surface availability of acid-base adsorption sites on the catalytic behaviour, the rate of CO_2 conversion was normalized for each catalyst at a temperature as low as 200 °C (wherein the low activity allows to rule out any control exerted by possible diffusional phenomena), both with respect to the number of basic sites (from CO_2 uptake) and with respect to the number of acid sites (from NH_3 uptake), so determining turnover frequency values associated to the CO_2 conversion (TOF CO_2) and DME formation (TOF DME), respectively. As it is possible to argue from Fig. 3, similar values of TOF CO_2 and TOF DME allows a rational overview of the peculiar reactivity of the 3D-printed hybrid CuO-ZnO-ZrO_2/zeolite system, clearly pointing to the chemisorption capacity as the critical factor controlling the specific activity of the investigated sample. On the whole, this finding matches the evidence that the reactivity of the 3D sample basically depends on the surface availability of the C-containing surface intermediates, in turn proportional both to CO_2 desorbed from basic CO_2 activation sites at the metal-oxide(s) interface [18,19,21] and to ammonia desorbed mainly from Brønsted acidic sites, considered of primary catalytic importance in the MeOH-to-DME dehydration reaction [26,29]. Although necessary in the step of H_2 activation, less decisive appears the role of metallic Cu^0 sites on the catalytic reactivity, considering not only a similar copper surface exposure exhibited by the two differently prepared investigated samples (19.7–20.3 m^2/g, see Table 1), but also a stoichiometrically larger surface availability of activated hydrogen species in respect of the other intermediate species, prompted by the volumetric H_2/CO_2 feed ratio of 3–1.

Finally, in Fig. 4 the stability pattern over the 3D-printed hybrid catalyst is reported in terms of CO_2 conversion and DME yield as a function of the time on stream, evidencing an almost steady state during 5 days of experimental run. Considering that, under the adopted conditions, no coke or metal sintering have been ever detected over the "used" catalysts [51], this meaningful result reflects the effectiveness of matrix-like materials on the management of the water formed during reaction, which is considered the main factor affecting the catalyst lifetime in powdered catalysts [28,51].

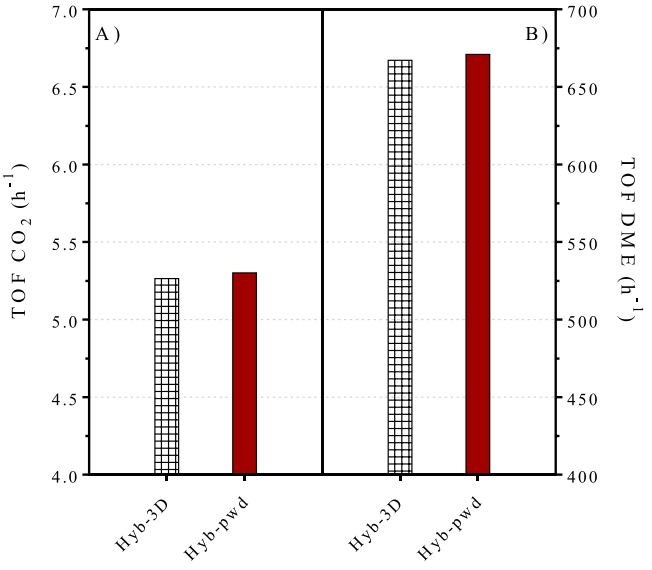

Fig. 3. Turnover frequency values of (A) CO_2 conversion (TOF CO_2) and (B) DME formation (TOF DME), as determined at T_R, 200 °C, P_R, 3.0 MPa, $CO_2/H_2/N_2$, 3/9/1 v/v; *GHSV*: 1000 *N*L/Kg_{cat}/h.

4. Conclusions

Once found the proper combination among ink-paste composition, 3D model and sintering treatments, the robocasting technique shows all its effectiveness, offering an alternative, cost-effective and facile approach to fabricate structured catalysts with tunable structural, chemical and morphological properties, comprehensively mirroring the features of conventional powdered catalysts used in CO_2 utilization technologies.

Probing the reactivity of a 3D-printed hybrid CuO-ZnO-ZrO_2/zeolite

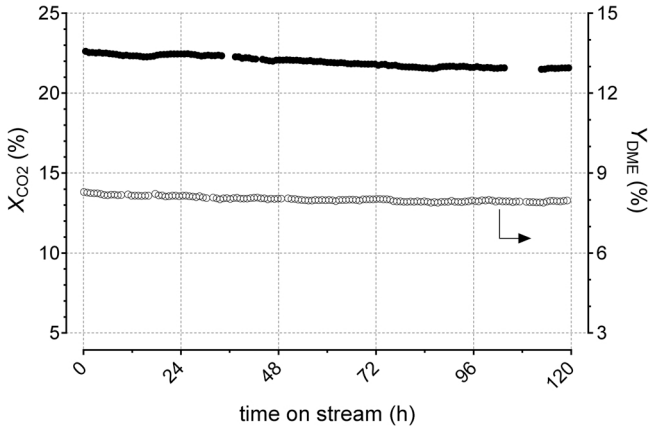

Fig. 4. Stability pattern of the Hyb-3D catalyst. Reaction conditions: P_R, 3.0 MPa; T_R, 260 °C; $CO_2/H_2/N_2$, 3/9/1 v/v; *GHSV*: 1000 *N*L/Kg_{cat}/h.

catalyst in the direct hydrogenation of CO_2 to DME, the activity-selectivity pattern was put in relation with the surface availability of acid-base adsorption sites, in turn controlled by the thermofluidic properties of the catalytic ink-paste prepared for the process of micro-extrusion. Considering the multi-site nature of the process considered, the specific functionality of 3D catalysts perfectly matches the behavior of the corresponding powdered counterparts only if a suitable exposure both of basic CO_2 activation sites at the metal-oxide(s) interface and acidic dehydration sites at the zeolite surface can be ensured, together determining the rate of formation/transformation of the C-containing surface intermediates.

This new knowledge ultimately informs process and equipment design for extrusion-based 3D-printing using not only ceramics but also hybridized catalytic ink-pastes, suggesting the need for an optimized setup capable of realizing structured systems with tailored chemico-physical properties.

CRediT authorship contribution statement

Giuseppe Bonura: Writing – review & editing, Funding acquisition, Supervision, Project administration. **Serena Todaro:** Investigation (XRF, XRD, BET, TPR, TPD) and Writing – original draft preparation; **Vesna Middelkoop:** Conceptualization, Funding acquisition, Project administration; **Yoran de Vos:** Formal analysis; **Hendrikus C.L. Abbenhuis:** Supervision; **Gijsbert Gerritsen:** Methodology; **Arjan J.J. Koekkoek:** Data curation; **Catia Cannilla:** Investigation (SEM measurements), Visualization; **Francesco Frusteri:** Writing – review & editing.

Declaration of Competing Interest

The authors declare that they have no known competing financial interests or personal relationships that could have appeared to influence the work reported in this paper.

Data Availability

Data will be made available on request.

Acknowledgements

This work is part of the CO2Fokus project which is supported by the European Union's Horizon 2020 Research and Innovation programme under Grant Agreement No. 838061. The authors would like to thank the EU Horizon 2020 Programme for this opportunity. This document reflects only the authors' view and the Innovation and Networks Executive Agency (INEA) and the European Commission are not responsible for any use that may be made of the information it contains.

References

[1] L. Zhang, Y. Song, J. Shi, Q. Shen, D. Hu, Q. Gao, W. Chen, K.-W. Kow, C. Pang, N. Sun, W. Wei, Adv. Atmos. Sci. 39 (2022) 1252–1270, https://doi.org/10.1007/s00376-022-1467-x.
[2] L. Jeffry, M.Y. Ong, S. Nomanbhay, M. Mofijur, M. Mubashir, P.L. Show, Fuel 301 (2021) 121017–121029, https://doi.org/10.1016/j.fuel.2021.121017.
[3] A.D.N. Kamkeng, M. Wang, J. Hu, W. Du, F. Qian, J. Chem. Eng. 409 (2021) 128138–128166, https://doi.org/10.1016/j.cej.2020.128138.
[4] X. Zheng, D. Streimikiene, T. Balezentis, A. Mardani, F. Cavallaro, H. Liao, J. Clean. Prod. 234 (2019) 1113–1132, https://doi.org/10.1016/j.jclepro.2019.06.140.
[5] H. Ishaq, C. Crawford, Fuel 331 (2023) 125684–125694, https://doi.org/10.1016/j.fuel.2022.125684.
[6] S. Saeidi, S. Najari, V. Hessel, K. Wilson, F.J. Keil, P. Concepción, S.L. Suib, A. E. Rodrigues, Prog. Energy Comb. Sci. 85 (2021) 100905–100968, https://doi.org/10.1016/j.pecs.2021.100905.
[7] A. Di Benedetto, A. Angelini, P. Stufano, J. Chem. Technol. Biotechnol. 89 (2014) 334–353, https://doi.org/10.1002/jctb.4229.
[8] M. Aresta, A.Di Benedetto, Dalton Trans 28 (2007) 2975–2992, https://doi.org/10.1039/B700658F.
[9] L. Song, H. Wang, S. Wang, Z. Qu, Appl. Cat. B 322 (2023) 122137–122147, https://doi.org/10.1016/j.apcatb.2022.122137.
[10] J. Wang, H. Liu, T. Wang, Y. Xi, P. Sun, F. Li, Catal. Today 410 (2023) 205–214, https://doi.org/10.1016/j.cattod.2022.05.034.
[11] M. Matzen, Y. Demirel, J. Clean. Prod. 139 (2016) 1068–1077, https://doi.org/10.1016/j.jclepro.2016.08.163.
[12] S.H. Park, C.S. Lee, Energy Convers. Manag 86 (2014) 848–863, https://doi.org/10.1016/j.enconman.2014.06.051.
[13] T.A. Semelsberger, R.L. Borup, H.L. Greene, J. Power Sources 156 (2006) 497–511, https://doi.org/10.1016/j.jpowsour.2005.05.082.
[14] G. Leonzio, J. CO2, Util 27 (2018) 326–354, https://doi.org/10.1016/j.jcou.2018.08.005.
[15] E. Catizzone, G. Bonura, M. Migliori, F. Frusteri, G. Giordano, Molecules 23 (2017) 31–58, https://doi.org/10.3390/molecules23010031.
[16] J. Sun, G. Yang, Y. Yoneyama, N. Tsubaki, A.C.S. Catal 4 (2014) 3346–3356, https://doi.org/10.1021/cs500967j.
[17] Z. Azizi, M. Rezaeimanesh, T. Tohidian, M.R. Rahimpour, Chem. Eng. Process. 82 (2014) 150–172, https://doi.org/10.1016/j.cep.2014.06.007.
[18] A. García-Trenco, A. Martínez, Appl. Catal. 411- 412 (2012) 170–179, https://doi.org/10.1016/j.apcata.2011.10.036.
[19] J.W. Bae, S.H. Kang, Y.J. Lee, K.W. Jun, Appl. Catal., B 90 (2009) 426–435, https://doi.org/10.1016/j.apcatb.2009.04.002.
[20] T.A. Semelsberger, R.L. Borup, H.L. Greene, J. Power Sources 156 (2006) 497–511, https://doi.org/10.1016/j.jpowsour.2005.05.082.
[21] N. Mota, E.M. Ordoñez, B. Pawelec, J.L.G. Fierro, R.M. Navarro, Catalysts 11 (2021) 411–444, https://doi.org/10.3390/catal11040411.
[22] K. Saravanan, Hyungwon Ham, Noritatsu Tsubaki, Jong Wook Bae, Appl. Catal., B 217 (2017) 494–522, https://doi.org/10.1016/j.apcatb.2017.05.085.
[23] G. Bonura, S. Todaro, L. Frusteri, I. Majchrzak-Kucęba, D. Wawrzyńczak, Z. Pászti, E. Tálas, A. Tompos, L. Ferenc, H. Solt, C. Cannilla, F. Frusteri, Appl. Catal., B 294 (2021) 120255–120264, https://doi.org/10.1016/j.apcatb.2021.120255.
[24] X. Guo, F. Liu, Y. Hua, H. Xue, J. Yu, D. Mao, G.L. Rempel, F.T.T. Ng, Catal. Today 407 (2023) 125–134, https://doi.org/10.1016/j.cattod.2022.02.004.
[25] A. Desgagnés, M.C. Iliuta, Chem. Eng. J. 454 (2023) 140214–140227, https://doi.org/10.1016/j.cej.2022.140214.
[26] E. Catizzone, C. Freda, G. Braccio, F. Frusteri, G. Bonura, J. Energy Chem. 58 (2021) 55–77, https://doi.org/10.1016/j.jechem.2020.09.040.
[27] S. Ren, X. Fan, Z. Shang, W.R. Shoemaker, L. Ma, T. Wu, S. Li, N.B. Klinghoffer, M. Yu, X. Liang, J. CO2, Util 36 (2020) 82–95, https://doi.org/10.1016/j.jcou.2019.11.013.
[28] G. Bonura, C. Cannilla, L. Frusteri, E. Catizzone, S. Todaro, M. Migliori, G. Giordano, F. Frusteri, Catal. Today 345 (2020) 175–182, https://doi.org/10.1016/j.cattod.2019.08.014.
[29] G. Bonura, M. Cordaro, C. Cannilla, A. Mezzapica, L. Spadaro, F. Arena, F. Frusteri, Catalysts 228 (2014) 51–57, https://doi.org/10.1016/j.cattod.2013.11.017.
[30] R. Khoshbin, M. Haghighi, Chem. Eng. Res. Des. 91 (2013) 1111–1122, https://doi.org/10.1016/j.cherd.2012.11.017.
[31] I. Sierra, J. Ereña, A. Aguayo, M. Olazar, J. Bilbao, Ind. Eng. Chem. Res. 49 (2009) 481–489, https://doi.org/10.1021/ie900978a.
[32] N. Erfani, D. Symons, C. Fee, M.J. Watson, Chem. Eng. Sci. 267 (2023) 118347–118364, https://doi.org/10.1016/j.ces.2022.118347.
[33] B. Guo, J. Guo, W. Yang, X. Tian, X. Wang, Z. Xiang, M. Wu, Renew, Energy 201 (2022) 117–124, https://doi.org/10.1016/j.renene.2022.11.036.
[34] W. Nie, W. Zhou, N. Li, M. Yuan, J. Yan, Y. Hua, Q. Bao, F. Yu, W. Niu, Catal. Lett. 152 (2022) 3642–3654, https://doi.org/10.1007/s10562-022-03922-7.
[35] E. Bekhradinassab, M. Haghighi, A. Tavakoli, M. Shabani, Energy Convers. Manag. 270 (2022) 116178–116195, https://doi.org/10.1016/j.enconman.2022.116178.
[36] R. Brackmann, C.A. Perez, M. Schmal, Int. J. Hydrog. Energy 39 (2014) 13991–14007, https://doi.org/10.1016/j.ijhydene.2014.07.027.
[37] F. Monnet, Y. Schuurman, F.J. Cadete Santos Aires, C. Mirodatos, Stud. Surf. Sci. Catal. 136 (2001) 171–176, https://doi.org/10.1016/S0167–2991(01)80299–8.
[38] M. Valentini, G. Groppi, C. Cristiani, M. Levi, E. Tronconi, P. Forzatti, Catal. Today 69 (2001) 307–314, https://10.1016/S0920–5861(01)00383–2.
[39] L. Chen, S. Zhou, M. Li, F. Mo, S. Yu, J. Wei, Catalysts 12 (2022) 1081–1092, https://doi.org/10.3390/catal12101081.
[40] X. Zhou, C. Liu, Adv. Funct. Mater. 27 (2017) 1701134–1701147, https://doi.org/10.1002/adfm.201701134.
[41] A. Lind, Ø. Vistad, M.F. Sunding, K.A. Andreassen, J. Hafizovic Cavka, C.A. Grande, Mater. Des. 187 (2020) 108377–108384, https://doi.org/10.1016/j.matdes.2019.108377.
[42] C. Parra–Cabrera, C. Achille, S. Kuhn, R. Ameloot, Chem. Soc. Rev. 47 (2018) 209–230, https://doi.org/10.1039/C7CS00631D.
[43] M. Nowakowska, A. Rokicińska, P. Kuśtrowski, P. Michorczyk, Ceram. Int. 49 (2023) 1902–1910, https://doi.org/10.1016/j.ceramint.2022.09.155.
[44] F. Magzoub, X. Li, J. Al–Darwish, F. Rezaei, A.A. Rownaghi, Appl. Catal., B 245 (2019) 486–495, https://doi.org/10.1016/j.apcatb.2019.01.008.
[45] L. Long, K. Xu, K.B. Tan, D. Cai, Y. Yang, S.–F. Zhou, G. Zhan, Chem. Eng. Sci. 266 (2023) 118278–118292, https://doi.org/10.1016/j.ces.2022.118278.
[46] C.J.C. Nocheseda, F.P. Liza, A.K.M. Collera, E.B. Caldona, R.C. Advincula, Addit. Manuf. 48 (2021) 102380–102389, https://doi.org/10.1016/j.addma.2021.102380.
[47] X. Zhou, C.J. Liu, Catal. Today 347 (2020) 2–9, https://doi.org/10.1016/j.cattod.2018.05.044.
[48] X. Li, F. Rezaei, A.A. Rownaghi, Microp. Mesop. Mater. 276 (2019) 1–12, https://doi.org/10.1016/j.micromeso.2018.09.016.

[49] V. Middelkoop, A. Vamvakeros, D. De Wit, S.D. Jacques, S. Danaci, C. Jacquot, Y. de Vos, D. Matras, S.Q.T. Price, A.M. Beale, J. CO2, Util 33 (2019) 478–487, https://doi.org/10.1016/j.jcou.2019.07.013.
[50] C.R. Tubío, J. Azuaje, L. Escalante, A. Coelho, F. Guitián, E. Sotelo, A. Gil, J. Catal 334 (2016) 110–115, https://doi.org/10.1016/j.jcat.2015.11.019.
[51] G. Bonura, M. Migliori, L. Frusteri, C. Cannilla, E. Catizzone, G. Giordano, F. Frusteri, J. CO_2 Util. 24 (2018) 398–406, https://doi.org/10.1016/j.jcou.2018.01.028.